LETTERS
https://doi.org/10.1038/s41566-018-0121-8

nature photonics

Corrected: Publisher correction

Spatiotemporal control of laser intensity

Dustin H. Froula[1,2*], David Turnbull[1], Andrew S. Davies[1,2], Terrance J. Kessler[1], Dan Haberberger[1], John P. Palastro[1], Seung-Whan Bahk[1], Ildar A. Begishev[1], Robert Boni[1], Sara Bucht[1,2], Joseph Katz[1] and Jessica L. Shaw[1]

The controlled coupling of a laser to plasma has the potential to address grand scientific challenges[1–6], but many applications have limited flexibility and poor control over the laser focal volume. Here, we present an advanced focusing scheme called a 'flying focus', where a chromatic focusing system combined with chirped laser pulses enables a small-diameter laser focus to propagate nearly 100 times its Rayleigh length. Furthermore, the speed at which the focus moves (and hence the peak intensity) is decoupled from the group velocity of the laser. It can co- or counter-propagate along the laser axis at any velocity. Experiments validating the concept measured subluminal (−0.09*c*) to superluminal (39*c*) focal-spot velocities, generating a nearly constant peak intensity over 4.5 mm. Among possible applications, the flying focus could be applied to a photon accelerator[7] to mitigate dephasing, facilitating the production of tunable XUV sources.

In conventional near-diffraction-limited systems, both the minimum focal-spot size ($w_0 \simeq f\lambda/2R$) and longitudinal focusing range ($Z_R \simeq (f/2R)^2\lambda$) are linked by the ratio of the focal length (f) to twice the radius of the beam (R). As a result, these systems require large laser spots to extend their focusing range or waveguides[8–11] to maintain small spots over long distances. At low energies, manipulation of the spatial phase has overcome this limitation[12,13], but a long focal range introduced in this way does not possess dynamic properties. Pulse front tilt was recently used to introduce a time-dependent rotation of the local wavefront in a scheme called the 'attosecond lighthouse'[14], but this lacked long longitudinal focusing range. The flying focus takes advantage of a temporally varying frequency (that is, chirp) and longitudinal chromatic focal dispersion to achieve a focusing range independent of the spot size, while also providing tunability of the focal-spot velocity. The flying focus presents an opportunity to extend interaction lengths and overcome current limitations in photon accelerators[7], laser–plasma amplifiers[15–18], laser–wakefield accelerators[19,20], high-order frequency conversion[21,22] and photon–electron light sources[23,24].

Figure 1 presents a schematic of the configuration that generates a flying focus. To produce a large chromatic focus while minimizing other aberrations, a diffractive lens with a radially varying groove density, $G = \frac{r}{\lambda_0 f_0}$, is used, where f_0 is the focal length of the system at the central wavelength λ_0, and r is the distance from the optical axis. With this lens, the longest wavelength (λ_r) focuses a length $L \simeq f_0 \frac{\Delta\lambda}{\lambda_0}$ before the shortest wavelength ($\lambda_b = \lambda_r - \Delta\lambda$). By introducing a laser pulse with a temporally varying wavelength, the focus will move at a velocity given by $v(z) = \mathrm{d}z/\mathrm{d}t$, where $\mathrm{d}z$ is the distance between two focused colours spectrally separated by $\delta\lambda$, $\mathrm{d}t = \mathrm{d}\tau + \mathrm{d}z/c$ is the time it takes for the two colours to reach their respective foci, $\mathrm{d}\tau$ is the time between the two colours ($\delta\lambda$) within the chirped laser pulse, and c is the speed of light. By changing the chirp of the laser beam, the time to reach focus for successive colours is varied to provide control of the focal velocity. In general, the velocity of the focus is given by

$$v(z)/c = \left[1 + \left(\frac{\mathrm{d}\lambda}{\mathrm{d}\tau}\right)^{-1}\left(\frac{\mathrm{d}z}{\mathrm{d}\lambda}\right)^{-1} c\right]^{-1} \quad (1)$$

where $\frac{\mathrm{d}z}{\mathrm{d}\lambda} \simeq -f_0/\lambda_0$ is the longitudinal dispersion provided by the diffractive lens and $\tau = t - z/c$. For a desired longitudinal focal-spot trajectory $z(t)$, a laser chirp can be designed, $\lambda(\tau)/\lambda_0 = [1 + z(\tau)/f_0]^{-1} \approx 1 - z(\tau)/f_0$. For a trajectory with a constant velocity, $z(t) = v_0 t$, a linear chirp is required, $\lambda(\tau) = (v_0\lambda_0/f_0)\tau + \lambda_{r,b}$, where $v_0 = L/T$, $\lambda_{r,b}$ is the initial wavelength, T is the chirped-pulse duration, and $|\tau| < T/2$.

Figure 2 shows measurements (see Methods for details) of the flying focus generated by negatively and positively chirped laser pulses, both with a duration of ~60 ps (see Supplementary Videos 1 and 2 for complete propagation across the focal regions). The initial frames show the laser beam entering the focal region. For the positively chirped case (Fig. 2, left), the beam has reached focus ($z \approx -2$ mm), and over the next ~60 ps the focal spot moves to the back of the focal region ($z \approx +2$ mm). This corresponds to a focal velocity of ~0.2*c*. This is in contrast to the negatively chirped case (Fig. 2, right) where the laser first comes to focus at the back of the focal region ($z \sim +2$ mm) and propagates to the front of the region over ~30 ps, corresponding to a velocity of about −0.5*c*.

Figure 3 shows the measured velocity of the focus as a function of the pulse duration of the laser. The measurements compare well with the calculations using equation (1). The results show that when the laser pulse was negatively chirped with a pulse duration of $T = 34$ ps, the focus counter-propagated at nearly the speed of light ($v = -0.87c \pm 2\%$). Reducing the pulse duration to $T = 19$ ps increased the counter-propagating superluminal focus to $v = -7.6c \pm 20\%$. A pulse duration of $T = 232$ ps generated a counter-propagating subluminal focus ($v/c \simeq -0.09 \pm 1\%$). Setting the pulse duration of the laser equal to the transit time of the light to propagate across the focal region ($T = L/c = 14.9$ ps) resulted in all of the colours focusing simultaneously, generating 4.5-mm-long line focus; from equation (1) this corresponds to an 'infinite' focal velocity. A positive chirp provides access to a range of forward-propagating subluminal velocities. The focal-spot velocity for a positively chirped laser pulse with a duration of $T = 65$ ps was measured to propagate at $v = 0.20c \pm 1\%$.

Figure 4 presents calculated snapshots of the longitudinal intensity profiles for three different negative chirp cases: propagating backwards at the speed of light (Fig. 4a), propagating instantaneously across the focal volume (Fig. 4b), and propagating forwards

[1]Laboratory for Laser Energetics, University of Rochester, Rochester, NY, USA. [2]Physics Department, University of Rochester, Rochester, NY, USA.
*e-mail: dustin.froula@rochester.edu

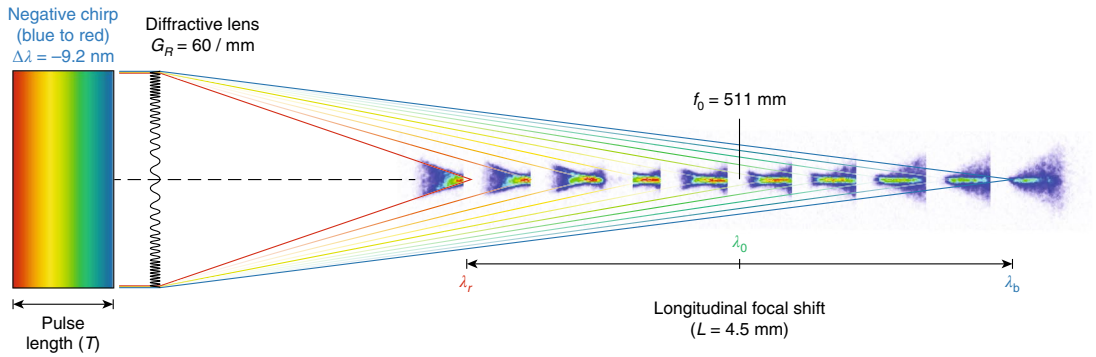

Fig. 1 | Schematic of the chromatic focusing system coupled to a chirped laser pulse. Measurements of temporal evolution of the intensity at various longitudinal locations along the focus. A negatively chirped pulse is shown where the colours change in time from blue to red. For a more complete visualization of the flying focus, see Supplementary Videos.

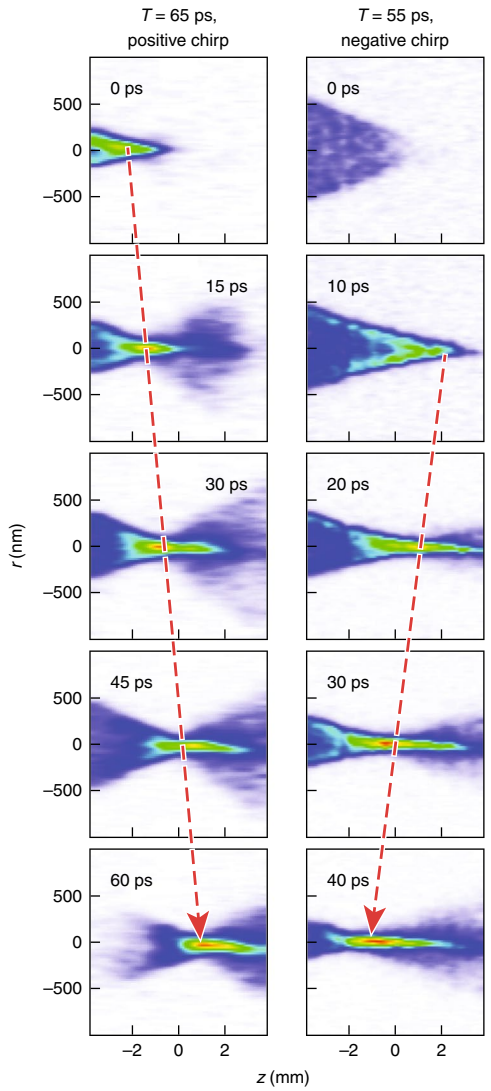

Fig. 2 | Evolution of the flying focus intensity. Left: evolution of intensity measured for a $T = 65$ ps positively chirped pulse. Right: evolution of intensity measured for a $T = 55$ ps negatively chirped pulse. The time relative to the first frame is written in each image. Dashed arrows show the initial to final focal spot location, indicating the direction of propagation. For the complete evolution, see Supplementary Videos 1 and 2.

faster than the speed of light (Fig. 4c) (see also corresponding Supplementary Videos 3, 4 and 5). These were calculated by assuming Gaussian optics, $\frac{I(z,t)}{I_0} = \left(\frac{w_0}{w(z,t)}\right)^2$, where $w_0 \simeq 1/2G_R$ is the diffraction-limited spot size and

$$w(z,t) \simeq w_0\sqrt{1+\frac{f_0^2}{4Z_R^2}\left[\frac{z}{f_0}-\frac{\lambda_0}{\lambda(\tau)}+1\right]^2} \quad (2)$$

is the radius of the flying focus spot. The Rayleigh length for a diffractive lens is given by $Z_R \simeq \frac{f_0^2\lambda_0}{4R^2} \simeq \frac{1}{4G_R^2\lambda_0} = 52\,\mu$m, where G_R is the groove density at the radius of the laser beam, R. This is a reasonable approach for calculating the intensity profile, provided that the pulse duration is much larger than the radial pulse front delay ($T > T_{RPFD} = 5$ ps). Chromatic aberration, whether from a conventional optic or the flying focus, leads to an extension of the focal region and an increase in the focal spot size when integrating over time. However, in the case of the flying focus, the instantaneous spot size at peak intensity is only increased by ~20% from a diffraction-limited focus. Furthermore, the small spot size is essentially constant over the longitudinal focal shift (L) (see Supplementary Section 'Flying Focus Spot Size').

In the regimes considered in this article, where the laser pulse duration is longer than the transform-limited duration (T_{tl}), the peak intensity is given in the standard way where the maximum laser intensity in a flying focus is nearly equivalent to a conventional system with the same incident power. Because the flying focus pulse is chirped, its duration is longer than a conventional system, requiring more energy to achieve the same intensity in the focal regimes ($I_0/I_{ff}E_0/E_{ff} = T/T_{tl}$). In practice, the additional energy is less constraining because the maximum energy in high-power laser systems is typically limited by peak power. Therefore, increasing the pulse duration allows the laser energy to be increased[25]. This is particularly relevant in glass laser systems (for example, the OMEGA EP and the MTW), where there is typically more stored energy than can be used at best compression. For example, in the MTW system, the maximum operational energy for a transform-limited pulse duration of ~1 ps is ~20 J, and when increasing the pulse duration to $T = 25$ ps, 110 J is achievable. This corresponds to a pulse counter-propagating at the speed of light over several millimetres with an intensity of $\sim 1 \times 10^{18}$ W cm^{-2}, which is a factor of about 5 lower peak intensity than achievable from a conventional focus.

The instantaneous longitudinal intensity profile can be controlled by spectrally shaping the laser pulse, $I(z,t) = \frac{P(\lambda)}{\pi[w(z,t)]^2}$. For

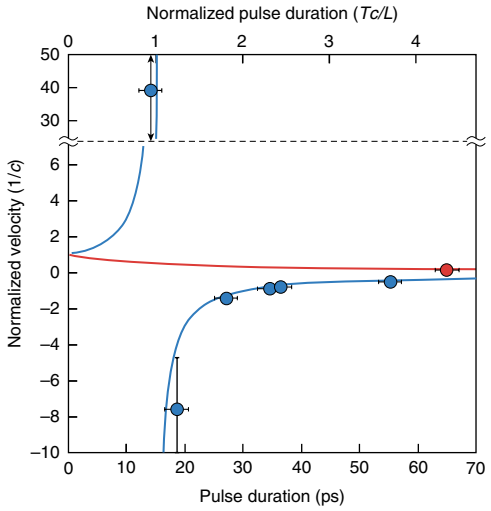

Fig. 3 | Measured and calculated $\left[v/c=\left(1\pm\frac{cT}{L}\right)^{-1}\right]$ focal-spot velocities plotted as a function of normalized laser pulse duration. Measured velocities are shown as points (bottom axis) and calculated velocities as curves (top axis). Red and blue symbols represent positively and negatively chirped laser pulse, respectively. For all but two of the data points, the error in the velocity measurements is smaller than the symbols (<2.5%). For the data point with a pulse duration of 14 ps (very close to L/c), error in the velocity measurement is large as the focal velocity is nearly 50 times the speed of light.

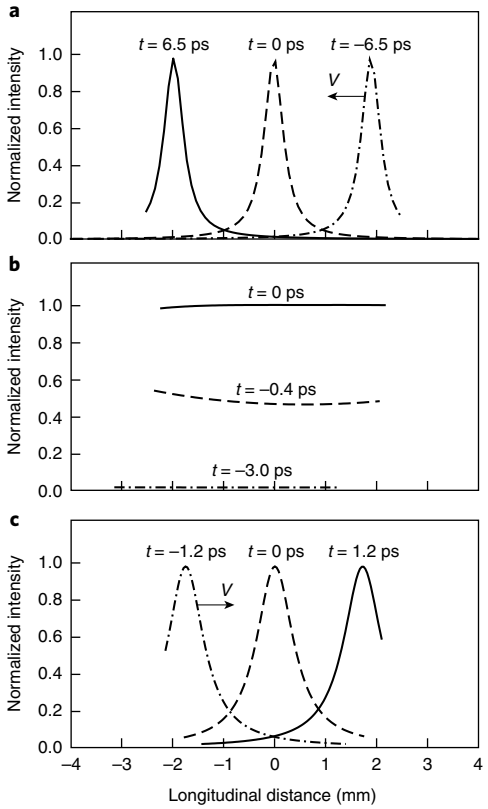

Fig. 4 | Instantaneous longitudinal intensity. a–c, Instantaneous longitudinal intensity plotted for a focus counter-propagating at the speed of light ($T=2L/c=29.8$ps, $\Delta\lambda=-9.2$ nm) (**a**), propagating at an 'infinite' velocity ($T=L/c=14.9$ ps, $\Delta\lambda=-9.2$ nm) (**b**) and co-propagating at five times the speed of light ($T=0.8L/c=11.9$ ps, $\Delta\lambda=-9.2$ nm) (**c**). Snapshots of the intensity profiles are taken at an early time (dotted–dashed curve), middle time (dashed curve) and late time (solid curve). Supplementary Videos 3, 4 and 5 correspond to the three examples shown.

example, modulating the spectral power will remove colours and reduce their overlapping power in the focal regime, narrowing the instantaneous intensity profile. This could be critical for applications that require a limited intensity profile or systems that require modulation of the longitudinal intensity. To demonstrate the effect of spectral power in the experiments, 1.6 nm of bandwidth was removed from the middle of a positively chirped spectrum. The measurements showed a gap in the central region of the longitudinal focus. The measured laser focus propagated subluminally ($v/c=0.16\pm1\%$) over the first ~2 mm and then did not focus again for ~26 ps, at which time the focus reappeared at $z\sim2.8$ mm and propagated to the end of the longitudinal focal region.

The flying focus provides an avenue for novel control of laser–plasma interactions, removes the need for long-focal-length systems or guiding structures to maintain high intensities over long distances, and decouples the velocity of the focal spot from the group velocity of the light. For more exotic applications, the velocity of the focus can be varied by using a nonlinear chirp and/or a nonlinear chromatic optical system. From equation (1) it is evident that the focal velocity could be made to accelerate, decelerate or oscillate across the longitudinal focal region depending on the design of the nonlinear chirp. For example, using a nonlinear chirp to accelerate the flying focus in phase with the increasing group velocity of photons in a photon accelerator could shift a conventional visible-wavelength laser into the extreme ultraviolet (XUV) or even the X-ray range while retaining the coherence, divergence, monochromacity and even polarization of the original source. Photons with an initial group velocity of $v_g=0.7c$ ($\lambda_0=1,054$ nm at $n_e=5\times10^{20}$ cm^{-3}) injected into the accelerator would accelerate to $v_g=0.99c$ ($\lambda'\simeq160$ nm) over 4.5 mm (see Supplementary section 'Photon Accelerator' for details).

In addition to photon accelerators, the spatiotemporal control of laser intensity achieved by the flying focus has the potential to change the way plasma and nonlinear optical devices are optimized and could be applied in many areas of physics. For applications that require a forward propagating pulse that significantly changes the refractive index, refraction could limit the intensity of the flying focus as subsequent colours come to focus[26], but for applications like terahertz generation in a nonlinear crystal[27], where the velocity of the flying focus is matched to the phase velocity of the emitted radiation ($v=v_{\mathrm{THz}}^{\mathrm{ph}}\approx2.2v_{\mathrm{op}}^{\mathrm{gr}}$, where $v_{\mathrm{op}}^{\mathrm{gr}}$ is the group velocity of optical light in the nonlinear crystal), the forward propagating focus is ideal. For applications where the group delay dispersion is significant, the laser chirp can be modified to compensate. In a laser–wakefield accelerator[28,29], the flying focus could eliminate dephasing by generating a focal spot that moves at a velocity that matches the accelerating electrons. Furthermore, a powerful characteristic of the flying focus with negative focal velocity is that each frequency focuses in front of the previously created plasma. This largely avoids laser–plasma interactions, which limit refraction and could be used to mitigate filamentation and stimulated scattering. For example, applying the flying focus to a laser–plasma amplifier could enable propagation of the pump laser over long distances while providing control of the plasma conditions observed by the seed and could be the enabling technology for an efficient laser–plasma amplifier [30].

Note added in proof: During the review of this manuscript, ref. [31] was published with a theoretical description of the flying focus, or in their words, the 'sliding focus', which was performed simultaneously and independently of our work.

Methods

Methods, including statements of data availability and any associated accession codes and references, are available at https://doi.org/10.1038/s41566-018-0121-8.

Received: 27 July 2017; Accepted: 5 February 2018;
Published online: 12 March 2018

References

1. Bulanov, S. S., Esirkepov, T. Z., Thomas, A. G. R., Koga, J. K. & Bulanov, S. V. Schwinger limit attainability with extreme power lasers. *Phys. Rev. Lett.* **105**, 220407 (2010).
2. Pellegrini, C. The history of X-ray free-electron lasers. *Eur. Phys. J. H* **37**, 659–708 (2012).
3. Joshi, C. et al. Ultrahigh gradient particle-acceleration by intense laser-driven plasma-density waves. *Nature* **311**, 525–529 (1984).
4. Corde, S. et al. Multi-gigaelectronvolt acceleration of positrons in a self-loaded plasma wakefield. *Nature* **524**, 442–445 (2015).
5. Yan, W. et al. High-order multiphoton Thomson scattering. *Nat. Photon* **11**, 514–520 (2017).
6. Malka, V. et al. Principles and applications of compact laser-plasma accelerators. *Nat. Phys.* **4**, 447–453 (2008).
7. Wilks, S. C., Dawson, J. M. & Mori, W. B. Frequency up-conversion of electromagnetic radiation with use of an overdense plasma. *Phys. Rev. Lett.* **61**, 337–340 (1988).
8. Durfee, C. G. & Milchberg, H. M. Light pipe for high intensity laser pulses. *Phys. Rev. Lett.* **71**, 2409–2412 (1993).
9. Jackel, S. et al. Channeling of terawatt laser-pulses by use of hollow wave-guides. *Opt. Lett.* **20**, 1086–1088 (1995).
10. Dorchies, F. et al. Monomode guiding of 10^{16} W/cm^2 laser pulses over 100 Rayleigh lengths in hollow capillary dielectric tubes. *Phys. Rev. Lett.* **82**, 4655–4658 (1999).
11. Froula, D. H. et al. Magnetically controlled plasma waveguide for laser wakefield acceleration. *Plasma Phys. Control. Fusion* **51**, 024009 (2009).
12. Wattellier, B., Sauteret, C., Chanteloup, J. C. & Migus, A. Beam-focus shaping by use of programmable phase-only filters: application to an ultralong focal line. *Opt. Lett.* **27**, 213–215 (2002).
13. Garcia-Guerrero, E. E., Mendez, E. R. & Escamilla, H. M. Design and fabrication of random phase diffusers for extending the depth of focus. *Opt. Express* **15**, 910–923 (2007).
14. Vincenti, H.,& Quéré, F. Attosecond lighthouses: how to use spatiotemporally coupled light fields to generate isolated attosecond pulses. *Phys. Rev. Lett* **108**, 113904 (2012).
15. Malkin, V. M., Shvets, G. & Fisch, N. J. Fast compression of laser beams to highly overcritical powers. *Phys. Rev. Lett.* **82**, 4448–4451 (1999).
16. Ren, J., Cheng, W., Li, S. & Suckewer, S. A new method for generating ultraintense and ultrashort laser pulses. *Nat. Phys.* **3**, 732–736 (2007).
17. Ping, Y. et al. Amplification of ultrashort laser pulses by a resonant Raman scheme in a gas-jet plasma. *Phys. Rev. Lett.* **92**, 175007 (2004).
18. Vieux, G. et al. An ultra-high gain and efficient amplifier based on Raman amplification in plasma. *Sci. Rep.* **7**, 2399 (2017).
19. Bingham, R. Plasma physics—surfing the wake. *Nature* **394**, 617–619 (1998).
20. Hooker, S. M. Developments in laser-driven plasma accelerators. *Nat. Photon.* **7**, 775–782 (2013).
21. Butler, A. et al. Demonstration of a collisionally excited optical-field-ionization XUV laser driven in a plasma waveguide. *Phys. Rev. Lett.* **91**, 205001 (2003).
22. Rocca, J. J. et al. Demonstration of a discharge pumped table-top soft-X-ray laser. *Phys. Rev. Lett.* **73**, 2192–2195 (1995).
23. Powers, N. D. et al. Quasi-monoenergetic and tunable X-rays from a laser-driven compton light source. *Nat. Photon.* **8**, 29–32 (2014).
24. Phuoc, K. T. et al. All-optical compton gamma-ray source. *Nat. Photon.* **6**, 308–311 (2012).
25. Stuart, B. C. et al. Laser-induced damage in dielectrics with nanosecond to subpicosecond pulses. *Phys. Rev. Lett.* **74**, 2248–2251 (1995).
26. Palastro, J. P. et al. Ionization waves of arbitrary velocity driven by a flying focus. *Phys. Rev. A* (in the press).
27. Kim, K. Y. et al. Coherent control of terahertz supercontinuum generation in ultrafast laser-gas interactions. *Nat. Photon.* **2**, 605–609 (2008).
28. Geddes, C. G. R. et al. High-quality electron beams from a laser wakefield accelerator using plasma-channel guiding. *Nature* **431**, 538–541 (2004).
29. Steinke, S. et al. Multistage coupling of independent laser-plasma accelerators. *Nature* **530**, 190–193 (2016).
30. Turnbull, D. et al. Raman amplification with a flying focus. *Phys. Rev. Lett.* **120**, 024801 (2018).
31. Sainte-Marie, A., Gobert, O. & Quere, F. Controlling the velocity of ultrashort light pulses in vacuum through spatio-temporal couplings. *Optica* **4**, 1298–1304 (2017).

Acknowledgements

The work published here was supported by the US Department of Energy Office of Fusion Energy Sciences under contract no. DE-SC0016253, the Department of Energy under cooperative agreement no. DE-NA0001944, the University of Rochester, and the New York State Energy Research and Development Authority. The support of the Department of Energy does not constitute an endorsement of the views expressed in this article.

Author contributions

D.H.F. contributed the concept of flying focus to the team. D.T. carried out the experiments and performed the data analysis. T.J.K. designed, tested and delivered the diffractive optic. D.H. oversaw the experimental area and contributed to the design. J.P.P. and S.-W.B. performed electromagnetic wave calculations of the flying focus. I.A.B. designed the chirp and operated the laser system. R.B. designed the experimental set-up. S.B., J.L.S. and J.K. set up the experiment. A.S.D. helped with the analytic calculations.

Competing interests

The authors declare no competing interests.

Additional information

Supplementary information is available for this paper at https://doi.org/10.1038/s41566-018-0121-8.

Reprints and permissions information is available at www.nature.com/reprints.

Correspondence and requests for materials should be addressed to D.H.F.

Publisher's note: Springer Nature remains neutral with regard to jurisdictional claims in published maps and institutional affiliations.

Methods

The multi-terawatt laser (MTW)[32] at the University of Rochester's Laboratory for Laser Energetics was used with low energies (<1 mJ) to demonstrate the flying focus concept. The system is a Nd:glass optical parametric chirped-pulse-amplification laser with a central wavelength of $\lambda_0 = 1{,}054$ nm. The bandwidth ($\Delta\lambda = 9.2$ nm full-width at 0.1-times maximum) was stretched and a set of compressor gratings subsequently compressed the pulse to the desired chirped-pulse duration. Under-compression relative to the transform-limited pulse duration resulted in a positive linear chirp ($\lambda(\tau) = \frac{\Delta\lambda}{T}\tau + \lambda_r$) and over-compression resulted in a negative linear chirp ($\lambda(\tau) = -\frac{\Delta\lambda}{T}\tau + \lambda_b$). A high-efficiency (99% into the first order) diffractive lens with a high wavefront quality and a focal length of $f_0 = 511$ mm (at λ_0) generated am approximately 15-μm-diameter focus with a longitudinal separation of $L \simeq 4.5$ mm between the extreme wavelengths. This focal region is nearly 100 times the Rayleigh length ($Z_R = 0.05$ mm) of the *f*/7 optical system.

The experiments (Supplementary Fig. 4) used a parallel path configuration where the collimated laser beam ($R = 3.5$ cm) was split into two identical beams to form signal and reference paths that were then imaged onto a P510 Rochester optical streak camera (ROSS). Inside one of the parallel paths, the signal path was focused by the diffractive lens ($f_0 = 550$ mm) and the reference path was focused by an achromatic lens with a focal length of 400 mm. Both paths used achromatic lenses ($f_{r,s} = 400$ mm; where r indicates reference and s indicates signal) to collimate the light, which was then recombined with a slight angle to separate the images at the detector plane. The beams were focused to the detectors with a final achromatic lens ($f_2 = 400$ mm) that produced an image of the reference and signal focal regions. Modelling indicated that the optical system was ~3× diffraction-limited (~15 μm) over the wavelength range of interest. The spatial resolution at the detector plane of the ROSS camera was ~50 μm full-width at half-maximum (FWHM). The reported pulse duration was determined using the reference pulse measured on the ROSS camera. The impulse response of the streak camera was measured to be 7 ps FWHM.

The diameter of the signal pulse as a function of longitudinal position z along the longitudinal focal length was determined by moving the collection lens (f_s) over successive positions spanning slightly beyond the range of extreme focal positions. At each z position, several images were recorded by the streak camera (Supplementary Fig. 1) and averaged to increase the signal-to-noise ratio. The reference pulse was used to remove jitter between images. Each composite image generated a measurement of the time between the reference pulse and the signal pulse (τ).

The velocity, $v = \Delta z/\Delta t = c\left(1 + \frac{\Delta\tau}{\Delta z}c\right)^{-1}$, was determined by measuring the time of the minimum diameter foci (τ) at each image plane (z). The slope of a best fit line to the measured data (Supplementary Fig. 1b) was used to determine $m = c\Delta\tau/\Delta z$. The error in the measurements shown in Fig. 3 is given by $\delta v/v = v\delta m$, where δm is the uncertainty in each fit. For all but two of the data points shown in Fig. 3, the error in the velocity measurements is extremely small (<2.5%). For the data point with a pulse duration of 14 ps (very close to L/c), the error in the velocity measurement is large as the focal velocity is nearly 50 times the speed of light.

Figure 2 was constructed from temporal measurements, similar to those shown in Supplementary Fig. 1, taken at 30 longitudinal locations ranging from $z = -3.75$ mm to $z = +3.75$ mm. Each measurement captures the spot size of the laser at a single point in space but at every point in time. Each data set consists of multiple images varying the image plane location in increments of Δz to measure different points in space. By dividing each image into bins of size $\Delta z/c$, the data were then regrouped into frames representing a single point in time but every point in space. Played forward in time, this yields a video of the laser propagating through the focal region, which highlights the focal spot dynamics (for example, Supplementary Videos 1 and 2). Several frames from the videos were used to construct Fig. 2.

Data availability. The data that support the plots within this paper and other findings of this study are available from the corresponding author upon reasonable request.

References

32. Bagnoud, V., Begishev, I. A., Guardalben, M. J., Puth, J. & Zuegel, J. D. 5-Hz, >250-mJ optical parametric chirped-pulse amplifier at 1053 nm. *Opt. Lett.* **30**, 1843–1845 (2005).